Acta Crystallographica Section F
Structural Biology and Crystallization Communications
ISSN 1744-3091

Cloning, overexpression, crystallization and preliminary X-ray crystallographic analysis of a slow-processing mutant of penicillin G acylase from *Kluyvera citrophila*

Nishant Kumar Varshney,[a]‡ Sureshkumar Ramasamy,[a,b]‡ James A. Brannigan,[c] Anthony J. Wilkinson[c] and C. G. Suresh[a]*

[a]Division of Biochemical Sciences, CSIR – National Chemical Laboratory, Pune 411 008, Maharashtra, India, [b]California Institute of Technology, Pasadena, USA, and [c]York Structural Biology Laboratory, University of York, Heslington, York YO10 5DD, England

‡ These authors made equal contributions.

Correspondence e-mail: cg.suresh@ncl.res.in

Received 14 May 2013
Accepted 14 July 2013

Kluyvera citrophila penicillin G acylase (*Kc*PGA) has recently attracted increased attention relative to the well studied and commonly used *Escherichia coli* PGA (*Ec*PGA) because *Kc*PGA is more resilient to harsh conditions and is easier to immobilize for the industrial hydrolysis of natural penicillins to generate the 6-aminopenicillin (6-APA) nucleus, which is the starting material for semi-synthetic antibiotic production. Like other penicillin acylases, *Kc*PGA is synthesized as a single-chain inactive pro-PGA, which upon autocatalytic processing becomes an active heterodimer of α and β chains. Here, the cloning of the *pac* gene encoding *Kc*PGA and the preparation of a slow-processing mutant precursor are reported. The purification, crystallization and preliminary X-ray analysis of crystals of this precursor protein are described. The protein crystallized in two different space groups, *P*1, with unit-cell parameters a = 54.0, b = 124.6, c = 135.1 Å, α = 104.1, β = 101.4, γ = 96.5°, and *C*2, with unit-cell parameters a = 265.1, b = 54.0, c = 249.2 Å, β = 104.4°, using the sitting-drop vapour-diffusion method. Diffraction data were collected at 100 K and the phases were determined using the molecular-replacement method. The initial maps revealed electron density for the spacer peptide.

1. Introduction

Almost 85% of global 6-aminopenicillanic acid (6-APA) production for the manufacture of semi-synthetic penicillins utilizes penicillin G acylase (PGA), an enzyme that hydrolyses (Fig. 1) penicillin G (benzyl penicillin). The majority of the enzyme is sourced from *Escherichia coli*. There is interest in PGA enzymes from other species, such as *Kluyvera citrophila* (*Kc*PGA), which tolerate harsher conditions such as higher temperatures, acid/alkaline pH and changes in solvent composition. These enzymes are easier to immobilize for applications in the pharmaceutical industry (Alvaro *et al.*, 1992; Fernandez-Lafuente *et al.*, 1991, 1996; Liu *et al.*, 2006). Improved industrial standards for the application of *Kc*PGA can be achieved by understanding the structure–activity relationship and protein stability and applying the insights obtained to protein engineering.

The maturation of inactive precursors through post-translational processing to obtain functional protein forms has long been known in viral proteins (Douglass *et al.*, 1984; Dougherty & Carrington, 1988), eukaryotic proteins such as prothrombin and meizothrombin (Petrovan *et al.*, 1998) and caspases (Stennicke & Salvesen, 1998). Although initially reported only in eukaryotes (Bussey, 1988), this was subsequently detected in prokaryotic systems such as *Bradyrhzobium japonicum* cytochrome bc_1 (Trumpower, 1990), *Bacillus subtilis* spore-coat proteins (Aronson *et al.*, 1989), *Bacillus polymyxa* amylase (Uozumi *et al.*, 1989), penicillin G acylases (PGAs; Thöny-Meyer *et al.*, 1992) and γ-glutamyltranspeptidase (Okada *et al.*, 2007).

The maturation pathway of PGA has been extensively studied for the *E. coli* ATCC 11105 enzyme (Böck *et al.*, 1983). The post-translational processing of PGA essentially consists of two steps: translocation of the precursor to the periplasmic membrane utilizing the twin arginine translocation (tat) machinery (Ignatova *et al.*, 2002) followed by autocatalytic intramolecular peptide-bond cleavage. This autocatalytic processing removes a 26-residue signal peptide and

a 54-residue linker peptide and results in the formation of active enzyme in the periplasm, which is a heterodimer of α and β chains of 209 and 557 amino-acid residues, respectively (Choi *et al.*, 1992; Böck *et al.*, 1983; Oh *et al.*, 1987). Basically identified as a member of the Ntn hydrolase superfamily (Brannigan *et al.*, 1995), *Kc*PGA, like *Ec*PGA, is translated as an inactive precursor (pre-pro-PGA). The overall sequence identity between *Ec*PGA and *Kc*PGA is 87% (α chain, 84.2%; β chain, 87.6%; spacer peptide, 90.7%). Cleavage of the Thr289–Ser290 bond leads to the unveiling of the primary amine group of Serβ1 (Ser290 of the precursor), creating the active centre in mature PGA. The rate-limiting step in the production of active enzyme is the intramolecular autoproteolytic processing of the precursor molecule and the final removal of the linker peptide (Kasche *et al.*, 1999; Hewitt *et al.*, 2000; Done *et al.*, 1998).

Lee *et al.* (2000) showed that *in vitro* processing of the precursor PGA from *E. coli* was analogous to that observed in *in vivo* studies and depended on the pH in the same manner, with an optimum processing pH in the physiological range 6.4–7.0. A sequence alignment of precursor proteins from four Gram-negative and two Gram-positive bacteria identified a conserved lysine residue (Lys299). Site-directed mutation of this Lys, which is sequentially close to the β-chain N-terminal serine residue (Ser290), and study using GST-precursor PGA fusion protein further confirmed that the Lys residue is the most probable candidate responsible for the pH-dependent activation. Therefore, activation may involve Lys299 and Ser290 as critical residues for autocatalytic processing of the PGA precursor (Lee *et al.*, 2000). These residues are also conserved in *Kc*PGA. The same mechanism, pH and temperature dependence of precursor autocatalytic processing to yield a processed form is known in other enzymes (Bron *et al.*, 1998; Little, 1993; Guan *et al.*, 1998). Understanding the three-dimensional structure of the precursor and processing intermediates may unravel the mechanism of action and the post-translational processing of the industrially useful *Kc*PGA enzyme.

2. Experimental methods

2.1. Site-directed mutagenesis and transformation

A 2562 bp PCR fragment covering the region 12 nucleotides upstream from the start codon of the *K. citrophila pac* gene and 12 nucleotides downstream was amplified using *K. citrophila* DMSZ 2660 (ATCC 21285) chromosomal DNA as a template, using primers designed according to the published coding sequence (Barbero *et al.*, 1986; accession No. M15418). Cleavage sites for the restriction endonucleases *Nde*I and *Xho*I, shown in bold, were included in the sense (5′-CAAGAGGAT**CATATG**AAAAATAGAAATCGTATG-ATCGTG-3′) and antisense (5′-GCCGAA**CTCGAG**GCGCTGTA-CCTGCAGCACTT-3′) primer sequences, respectively. The PCR products were digested using the corresponding restriction enzymes, purified by gel electrophoresis and inserted into the plasmid pET26b(+) (EMD Biosciences/Novagen, USA). The ligation products were used to transform NovaBlue competent cells resistant to kanamycin. Recombinant plasmids were isolated and their sequencing confirmed the success of the cloning experiment. This plasmid pET26-*Kc*PGA was then used as a template for the preparation of the mutant Ser290Gly (Serβ1Gly) using the Quik-Change site-directed mutagenesis kit (Stratagene, USA). Forward sense (5′-CTACCCGACCACT**G**GCAATATGTGGGTG-3′) and reverse antisense (5′-CACCCACATATTGC**C**AGTGGTCGGGT-AG-3′) primers were used for mutagenesis, with the site of mutation shown in bold. The mutagenesis products were used to transform *E. coli* NovaBlue cells and the presence of the desired mutations was confirmed by DNA sequencing.

2.2. Expression and purification

For expression and purification, the expression plasmid pET26-*Kc*PGA (S290G) was introduced into *E. coli* BL21 (DE3) pLysS cells. The transformed *E. coli* cells were cultured in 2×YT (yeast extract and tryptone) medium supplemented with 35 µg ml^{-1} kanamycin. The bacterial cells were grown at 310 K with shaking at 250 rev min^{-1} until the OD_{600} reached 0.8. Isopropyl β-D-1-thiogalactopyranoside (IPTG; Anatrace, USA) was added to the culture to a final concentration of 0.3 m*M* for induction. The N-terminally His-tagged Serβ1Gly mutant precursor protein was expressed by extending the culture time by an additional 3 h at 310 K with shaking at 250 rev min^{-1}.

The cells were harvested by centrifugation (Beckman/Coulter Avanti J-26XP) at 5000 rev min^{-1} and 277 K for 30 min. The cell pellet was resuspended in cold lysis buffer consisting of 50 m*M* Na HEPES pH 7.5, 50 m*M* NaCl, 10 m*M* β-mercaptoethanol, 30 m*M* imidazole and the cells were lysed by passage through a microfluidizer (Microfluidics, USA) three times. Cell debris was removed by centrifugation at 18 000*g* (Beckman/Coulter Avanti J-26XP) for 20 min at 277 K. A typical nickel-affinity chromatography method was applied for preliminary purification of the mutant precursor protein. The supernatant was loaded onto 5 ml Ni–NTA affinity resin (Qiagen, Germany) pre-equilibrated in lysis buffer. After extensively

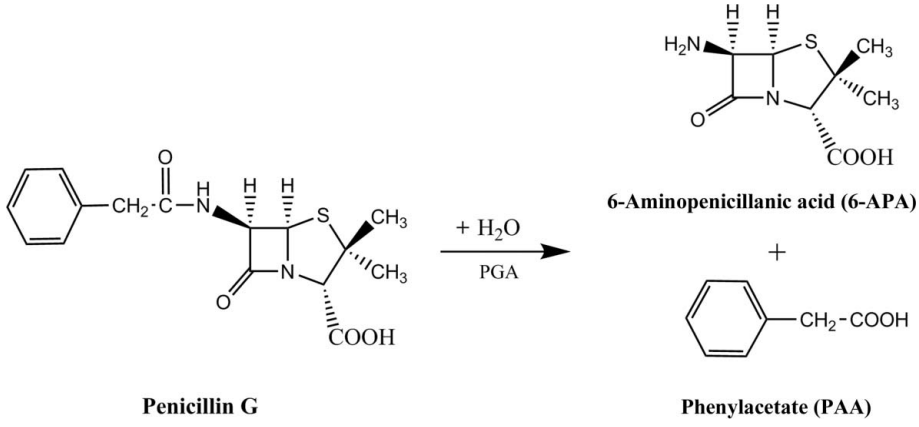

Figure 1
Hydrolysis of penicillin G (benzyl penicillin) by penicillin G acylase (PGA).

washing the resin with lysis buffer, the bound protein was eluted with elution buffer consisting of 50 m*M* Na HEPES pH 7.5, 50 m*M* NaCl, 300 m*M* imidazole. Fractions containing mutant protein were identified by 12% SDS–PAGE, pooled and concentrated by centrifugation (Amicon Ultra, Millipore, USA). The protein was further purified by size-exclusion chromatography on a Superdex 200 16/60 column (GE Healthcare, USA) with 50 m*M* Na HEPES pH 7.5, 50 m*M* NaCl, 1 m*M* DTT as the mobile phase. The purified mutant precursor protein was concentrated to 45 mg ml^{-1} in the same buffer for crystallization trials. The purified protein was found to be highly soluble and could be concentrated to more than 50 mg ml^{-1} without visible precipitation. The preparation mainly contained the unprocessed precursor PGA protein with molecular weight ∼92 kDa as seen on the SDS–PAGE gel (Fig. 2).

2.3. Crystallization and data collection

Since the Ser290Gly mutant is a slow-processing precursor, crystallization experiments were set up immediately after purification. Trials were conducted at 293 K using the vapour-diffusion method with sitting drops consisting of 300 nl protein solution (45 mg ml^{-1}) mixed with 300 nl reservoir solution and equilibrated against 100 µl reservoir solution. The screens were set up using a Mosquito crystallization robot (TTP LabTech, UK) as sitting-drop vapour-diffusion experiments in 96-well MRC plates (Hampton Research). Commercial crystallization kits from Hampton Research, Molecular Dimensions, Emerald BioSystems and Qiagen and self-prepared in-house screens were employed in the screening experiments. Crystals appeared in one of the self-prepared matrix screens. Multiple thin plate-like crystals were observed in 30%(*w*/*v*) PEG 4000, 50 m*M* sodium cacodylate pH 5.6, 0.5 *M* potassium thiocyanate in 3–4 d. Variation of the pH using similar protein-sample and precipitant concentrations in drops consisting of 500 nl protein solution and 500 nl well solution set up by a Gryphon crystallization robot (Art Robbins Instruments, USA) resulted in crystals that grew in a week under a wide range of pH conditions using 50 m*M* sodium cacodylate buffer. The crystals obtained at pH 4.6 and 6.5 diffracted and had a similar morphology (Fig. 3). These crystals were transferred into a cryoprotectant solution composed of the reservoir solution containing 30% glycerol and were flash-cooled in a nitrogen stream at 100 K. Diffraction data were collected at 100 K on beamline BL12-2 at the SLAC National Accelerator Laboratory at the Stanford Synchrotron Radiation Lightsource (SSRL). Diffraction images were collected on a DECTRIS PILATUS 6M detector.

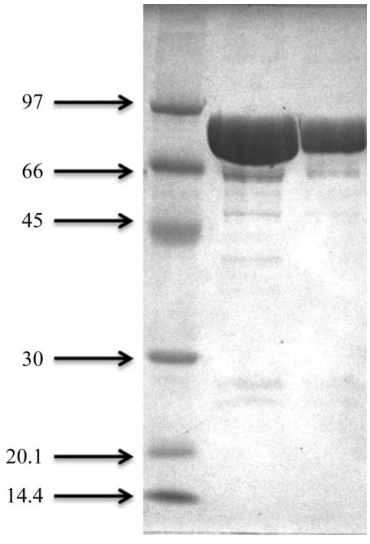

Figure 2
Coomassie-stained SDS–PAGE of the slow-processing *Kc*PGA Serβ1Gly mutant following electrophoresis. Left lane, Bio-Rad low-range marker (labelled in kDa); middle lane, precursor protein after fractionation on a nickel chelation column; right lane, precursor protein after further purification by size-exclusion chromatography.

3. Results and discussion

The slow-processing mutant precursor of *Kc*PGA (92 kDa) was purified using previously described protocols. The purity was checked using SDS–PAGE (Fig. 2), which showed a major band corresponding to pure precursor protein. Optimization of the crystallization conditions resulted in crystals that grew at two different pH values: 4.6 and 6.5 (Fig. 3). Diffraction data collected from these crystals were integrated using *XDS* (Kabsch, 2010) and scaled with *SCALA* in the *CCP*4 suite (Winn *et al.*, 2011). Based on the diffraction pattern, the two crystals obtained at pH 4.6 and 6.5 were indexed in different space groups. The crystals grown at pH 4.6 belonged to the triclinic space group *P*1, with unit-cell parameters a = 54.0, b = 124.6, c = 135.1 Å, α = 104.0, β = 101.4, γ = 96.5°, and diffracted to 2.5 Å resolution, whereas crystals obtained at pH 6.5 belonged to the monoclinic space group *C*2, with unit-cell parameters a = 265.1, b = 54.0, c = 249.2 Å, β = 104.4°, and diffracted to 3.5 Å resolution

(*a*)

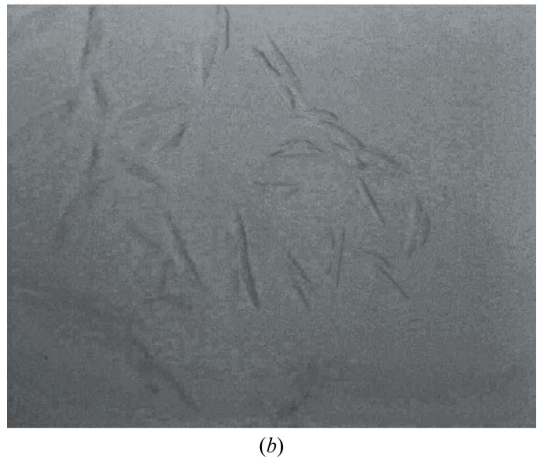

(*b*)

Figure 3
Crystals of the slow-processing Serβ1Gly mutant. They appeared within a week after setting up the drop. (*a*) Crystals of *Kc*PGA obtained at the low pH of 4.6 (space group *P*1) as observed using a microscope. The maximum size of the largest crystal is 200 µm. (*b*) Crystals of *Kc*PGA obtained at the higher pH of 6.5 (space group *C*2) as observed using a Rigaku crystal imager. The maximum size of the largest crystal is only 80 µm.

Table 1
Data-collection and processing statistics for the two crystal forms of the slow-processing mutant of *Kc*PGA.

Values in parentheses are for the outermost resolution shell.

Space group	*P*1	*C*2
Temperature (K)	100	100
X-ray source	BL12-2, SSRL	BL12-2, SSRL
Wavelength (Å)	0.9560	0.9560
Unit-cell parameters (Å, °)	a = 54.0, b = 124.6, c = 135.1, α = 104.1, β = 101.4, γ = 96.5	a = 265.1, b = 54.0, c = 249.2, β = 104.4
Molecules per asymmetric unit	4	4
Matthews coefficient (Å^3 Da^{-1})	2.48	2.51
Solvent content (%)	50	51
Total No. of observations	148560	125434
No. of unique observations	87317	42189
Multiplicity	1.7 (1.6)	3.0 (3.1)
Resolution range (Å)	38.6–2.5 (2.6–2.5)	38.8–3.5 (3.7–3.5)
Average $I/\sigma(I)$	6.1 (1.2)	4.0 (2.8)
$R_{\rm merge}$† (%)	9.5 (55.1)	26.1 (40.5)
$R_{\rm meas}$‡ (%)	13.4 (78.0)	31.7 (48.9)
$R_{\rm p.i.m.}$§ (%)	9.5 (55.1)	17.8 (27.1)
$CC_{1/2}$	98.9 (59.9)	94.1 (78.5)
Completeness (%)	76.5 (80.6)	96.0 (96.5)

† $R_{\rm merge} = \sum_{hkl}\sum_i |I_i(hkl) - \langle I(hkl)\rangle| / \sum_{hkl}\sum_i I_i(hkl)$. ‡ $R_{\rm meas} = \sum_{hkl}\{N(hkl)/[N(hkl)-1]\}^{1/2}\sum_i |I_i(hkl) - \langle I(hkl)\rangle| / \sum_{hkl}\sum_i I_i(hkl)$. § $R_{\rm p.i.m.} = \sum_{hkl}\{1/[N(hkl)-1]\}^{1/2}\sum_i |I_i(hkl) - \langle I(hkl)\rangle| / \sum_{hkl}\sum_i I_i(hkl)$.

(Fig. 4). As the molecular weight of the PGA precursor is 92 kDa, the Matthews coefficients calculated for four molecules in the asymmetric unit for the *P*1 and *C*2 crystals were 2.48 and 2.51 Å^3 Da^{-1}, respectively, corresponding to solvent contents of 50 and 51% (Matthews, 1968). The data-collection and processing statistics for both crystals are summarized in Table 1.

Reflections from the two crystal forms were phased using the molecular-replacement (MR) method. The structure of the *Ec*PGA precursor (PDB entry 1e3a; Hewitt *et al.*, 2000), which is the closest structure to *Kc*PGA, was used as the search model for both data sets. The *AutoMR* program from *PHENIX* (Adams *et al.*, 2002; McCoy *et al.*, 2007) was used for MR calculations. Executing the *PHENIX AutoMR* wizard (Adams *et al.*, 2002) in default mode with 1e3a as a template resulted in a single solution with an LLG gain of 9234.9, a rotation-function *Z* (RFZ) score of 10.1 and a translation-function *Z* (TFZ) score of 50.8 for the *P*1 data set. Similarly, an MR solution was obtained with the same program suite for the *C*2 data set. The LLG gain, RFZ and TFZ scores in this case were 2278.0, 17.1 and 15.9, respectively. A TFZ score above 8 usually indicates a correct structure solution (McCoy *et al.*, 2007). A non-origin Patterson peak one-quarter the height of the origin peak that was found in the case of the *C*2 data set may indicate the presence of pseudo-translational noncrystallographic symmetry (NCS). A pseudo-translational NCS vector was found at 0.2451, 0.2576 and 0.4973. The initial phases obtained from MR were sufficient for automatic tracing of the protein structure and preliminary model building. Automatic rebuilding was performed using the *AutoBuild* wizard (Terwilliger *et al.*, 2008) from *PHENIX*, unchecking the option of adding water molecules. *AutoBuild* combines density modification and chain tracing using *RESOLVE* (Terwilliger, 2000) and refinement using *phenix.refine* (Afonine *et al.*, 2005) to generate a high-quality model. Automated model building and refinement using *AutoBuild* built four molecules, each comprising 3272 of the total 3312 residues of the complete chain (including the hexahistidine tag), in the asymmetric unit with $R_{\rm cryst}$ and $R_{\rm free}$ values of 22.9 and 27.5%, respectively, for the *P*1 data set; the same 3272 residues were built for the *C*2 data set with $R_{\rm cryst}$ and $R_{\rm free}$ values of 35.0 and 42.0%, respectively, yielding sufficiently informative electron-density maps to evaluate the model. The default values in *phenix.refine* (5% of the data) were used to calculate $R_{\rm free}$. Initial electron-density maps calculated using data from each of the two crystal forms revealed density for amino acids 236–289 corresponding to the spacer peptide of the *Kc*PGA precursor (Fig. 5). This is further confirmed by OMIT maps. The presence of electron density for the spacer, along with molecular-weight determination under denaturing conditions, confirms that the precursor form of the molecule has crystallized, although the mutant is known to undergo slow autocatalytic processing. Since the *C*2 data have poor resolution and the *P*1 data have poor completeness owing to rapid radiation

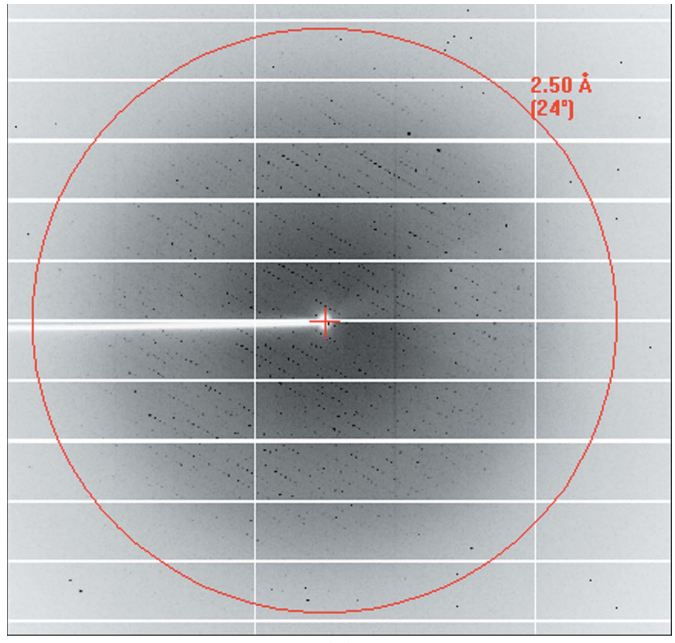

(*a*)

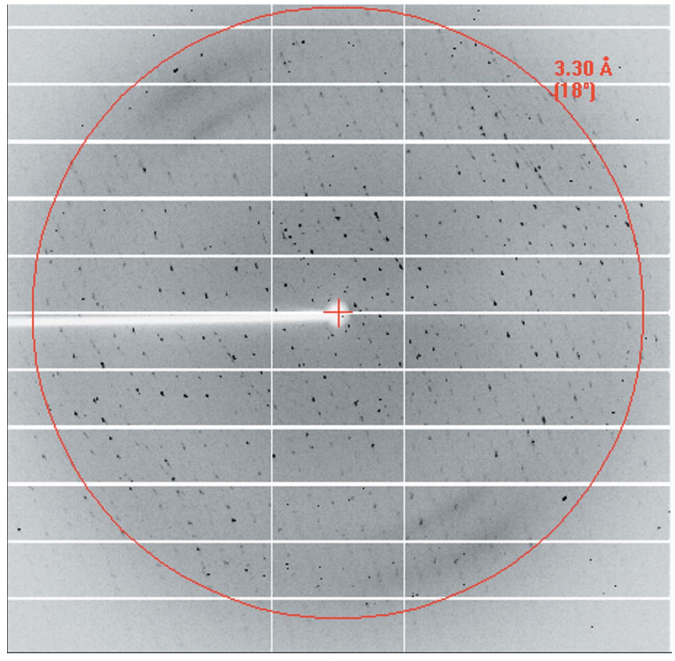

(*b*)

Figure 4
X-ray diffraction patterns obtained from crystals of the *Kc*PGA mutant precursor crystals (*a*) in space group *P*1 and (*b*) in space group *C*2. The numbering on the rings indicates the resolution of the data. The spots at the edges could be owing to buffer/salt.

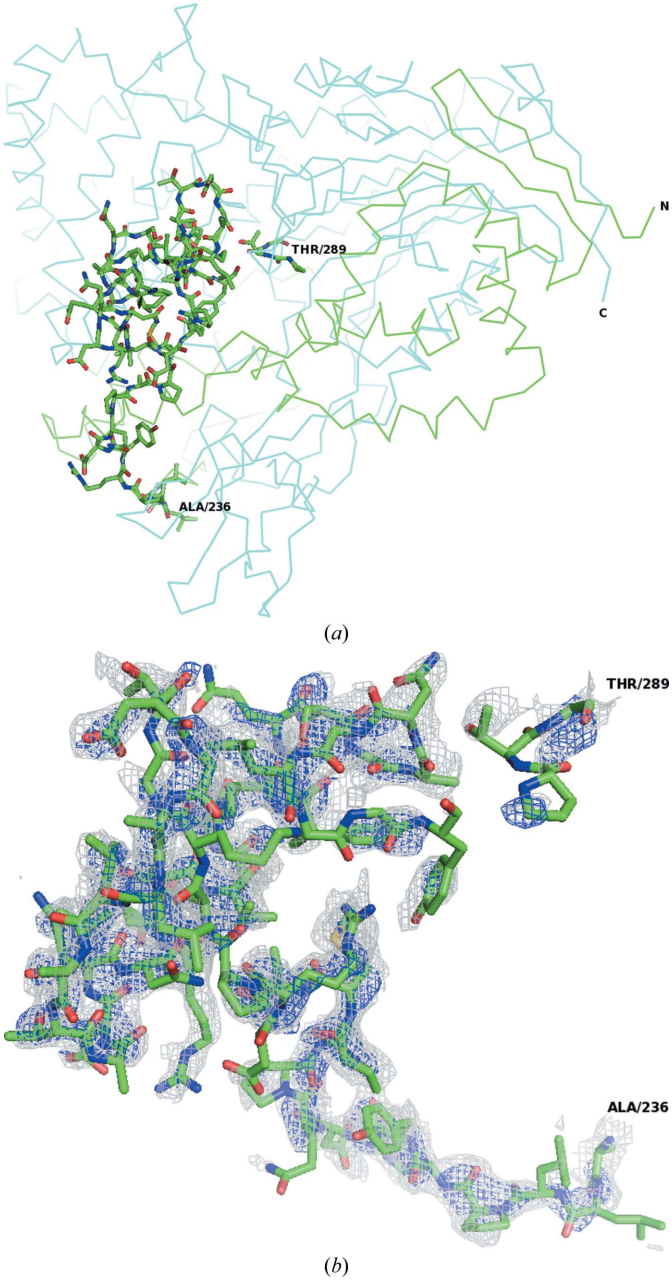

Figure 5
(*a*) The model of *Kc*PGA shown was obtained after carrying out MR calculations and the first cycle of refinement. The spacer peptide is highlighted and the rest of the molecule is shown as a C^{α} trace. The N- and C-termini are labelled. (*b*) The spacer peptide is shown overlapping with $2F_o - F_c$ (grey colour, 1σ level) and $F_o - F_c$ (blue, 3σ) maps. This figure was prepared using *PyMOL* v.1.5.0.2 (Schrödinger LLC.).

damage, neither could be used for complete refinement. Efforts are ongoing to achieve higher resolution and complete data.

NKV thanks the Council of Scientific and Industrial Research (CSIR, India) for a research fellowship and the Commonwealth Scholarship Commission, UK and the British Council, UK for a split-site PhD scholarship. SR thanks the staff at SSRL beamline 12-2 for help with data collection. Operations at SSRL are supported by the US DOE and NIH. The authors thank Ranu Sharma for help in drawing Fig. 1.

References

Adams, P. D., Grosse-Kunstleve, R. W., Hung, L.-W., Ioerger, T. R., McCoy, A. J., Moriarty, N. W., Read, R. J., Sacchettini, J. C., Sauter, N. K. & Terwilliger, T. C. (2002). *Acta Cryst.* D**58**, 1948–1954.
Afonine, P. V., Grosse-Kunstleve, R. W. & Adams, P. D. (2005). *Acta Cryst.* D**61**, 850–855.
Alvaro, G., Fernandez-Lafuente, R., Rosell, C. M., Blanco, R. M., Garcia-Lopez, J. L. & Guisan, J. M. (1992). *Biotechnol. Lett.* **14**, 285–290.
Aronson, A. I., Song, H.-Y. & Bourne, N. (1989). *Mol. Microbiol.* **3**, 437–444.
Barbero, J. L., Buesa, J. M., González de Buitrago, G., Méndez, E., Péz-Aranda, A. & García, J. L. (1986). *Gene*, **49**, 69–80.
Böck, A., Wirth, R., Schmid, G., Schumacher, G., Lang, G. & Buckel, P. (1983). *FEMS Microbiol. Lett.* **20**, 135–139.
Brannigan, J. A., Dodson, G., Duggleby, H. J., Moody, P. C., Smith, J. L., Tomchick, D. R. & Murzin, A. G. (1995). *Nature (London)*, **378**, 416–419.
Bron, S., Bolhuis, A., Tjalsma, H., Holsappel, S., Venema, G. & van Dijl, J. M. (1998). *J. Biotechnol.* **64**, 3–13.
Bussey, H. (1988). *Yeast*, **4**, 17–26.
Choi, K. S., Kim, J. A. & Kang, H. S. (1992). *J. Bacteriol.* **174**, 6270–6276.
Done, S. H., Brannigan, J. A., Moody, P. C. & Hubbard, R. E. (1998). *J. Mol. Biol.* **284**, 463–475.
Dougherty, W. G. & Carrington, J. C. (1988). *Annu. Rev. Phytopathol.* **26**, 123–143.
Douglass, J., Civelli, O. & Herbert, E. (1984). *Annu. Rev. Biochem.* **53**, 665–715.
Fernandez-Lafuente, R., Rosell, C. M. & Guisán, J. M. (1991). *Enzyme Microb. Technol.* **13**, 898–905.
Fernandez-Lafuente, R., Rosell, C. M. & Guisán, J. M. (1996). *Biotechnol. Appl. Biochem.* **2**, 139–143.
Guan, C., Liu, Y., Shao, Y., Cui, T., Liao, W., Ewel, A., Whitaker, R. & Paulus, H. (1998). *J. Biol. Chem.* **273**, 9695–9702.
Hewitt, L., Kasche, V., Lummer, K., Lewis, R. J., Murshudov, G. N., Verma, C. S., Dodson, G. G. & Wilson, K. S. (2000). *J. Mol. Biol.* **302**, 887–898.
Ignatova, Z., Hörnle, C., Nurk, A. & Kasche, V. (2002). *Biochem. Biophys. Res. Commun.* **291**, 146–149.
Kabsch, W. (2010). *Acta Cryst.* D**66**, 125–132.
Kasche, V., Lummer, K., Nurk, A., Piotraschke, E., Rieks, A., Stoeva, S. & Voelter, W. (1999). *Biochim. Biophys. Acta*, **1433**, 76–86.
Lee, H., Park, O. K. & Kang, H. S. (2000). *Biochem. Biophys. Res. Commun.* **272**, 199–204.
Little, J. W. (1993). *J. Bacteriol.* **175**, 4943–4950.
Liu, S.-L., Wei, D.-Z., Song, Q.-X., Zhang, Y.-W. & Wang, X.-D. (2006). *Bioprocess Biosyst. Eng.* **28**, 285–289.
McCoy, A. J., Grosse-Kunstleve, R. W., Adams, P. D., Winn, M. D., Storoni, L. C. & Read, R. J. (2007). *J. Appl. Cryst.* **40**, 658–674.
Matthews, B. W. (1968). *J. Mol. Biol.* **33**, 491–497.
Oh, S.-J., Kim, Y.-C., Park, Y.-W., Min, S.-Y., Kim, I.-S. & Kang, H.-S. (1987). *Gene*, **56**, 87–97.
Okada, T., Suzuki, H., Wada, K., Kumagai, H. & Fukuyama, K. (2007). *J. Biol. Chem.* **282**, 2433–2439.
Petrovan, R. J., Govers-Riemslag, J. W. P., Nowak, G., Hemker, H. C., Tans, G. & Rosing, J. (1998). *Biochemistry*, **37**, 1185–1191.
Stennicke, H. R. & Salvesen, G. S. (1998). *Biochim. Biophys. Acta*, **1387**, 17–31.
Terwilliger, T. C. (2000). *Acta Cryst.* D**56**, 965–972.
Terwilliger, T. C., Grosse-Kunstleve, R. W., Afonine, P. V., Moriarty, N. W., Zwart, P. H., Hung, L.-W., Read, R. J. & Adams, P. D. (2008). *Acta Cryst.* D**64**, 61–69.
Thöny-Meyer, L., Böck, A. & Hennecke, H. (1992). *FEBS Lett.* **307**, 62–65.
Trumpower, B. L. (1990). *Microbiol. Mol. Biol. Rev.* **54**, 101–129.
Uozumi, N., Sakurai, K., Sasaki, T., Takekawa, S., Yamagata, H., Tsukagoshi, N. & Udaka, S. (1989). *J. Bacteriol.* **171**, 375–382.
Winn, M. D. *et al.* (2011). *Acta Cryst.* D**67**, 235–242.